communications earth & environment

Article

https://doi.org/10.1038/s43247-024-01606-1

Hot springs reflect the flooding of slab-derived water as a trigger of earthquakes

Check for updates

Tsutomu Yamanaka [1] ✉ & Ikuya Adachi[2]

In subduction zones, water expelled from the subducting slab is believed to be involved in seismic activity. However, little is known about its quantity and flow processes. Here, we show that the Arima hot springs in western Japan contain high concentrations of water derived from the subducting Philippine Sea slab. A long-term record spanning over half a century reveals that the fraction of slab-derived water exhibited a temporary surge in the year preceding and/or subsequent years of the 1995 Kobe (Hyogo-ken Nanbu) earthquake. In total, an estimated 2.6–4.2 × 10^5 cubic meters of slab-derived water was introduced in conjunction with the earthquake. We infer that the earthquake was triggered by a flood-like release of water from the slab or by the bursting of clogged flow paths to the hypocenter. Our findings highlight the importance of hydrologically slab-connected hot springs for understanding ultradeep water cycles and their causal relationships with seismic phenomena.

Water is a key substance not only on Earth's surface but also in its interior. The oceanic plate and overlying sediments contain free water in pore spaces and bound water (or in the form of hydroxyl OH) in hydrous minerals[1]. In subduction zones, water contained in subducting slabs is expelled by compaction and dehydration processes, constituting a deep water cycle that is pivotal for earthquake occurrence as well as arc magmatism[2–4]. Based mainly on seismic data analyses, many studies have revealed the involvement of deep fluids in nonvolcanic earthquakes[5,6], and some of them interpret deep fluids as slab-derived[7–10]. However, in the case of an earthquake swarm for the years preceding the main shock of the 2024 Noto Peninsula earthquake (M_w7.5) that struck Japan on New Year's Day, it is controversial whether the origin of such fluids (and water) was a slab[11], uppermost mantle[12], or hidden magma[13]. Moreover, while progress has been made in quantifying the amount of water transported to the mantle by subducting slabs, the mechanism and location of water release from the slabs as well as the amount and flow paths of the released water remain unclear[14].

Here, we target nonvolcanic hot springs at Arima, a renowned spa area with a history of more than a millennium, in western Japan (Fig. 1, Supplementary Table 1). The hot spring water called 'Arima-type (deep) brine', which is characterized by unique H and O isotopic signatures (expressed as δ^2H and δ^{18}O) that are clearly distinct from those of meteoric water and a high Cl content of more than twice that of seawater[15,16], is considered to contain slab-derived water[17,18]. In addition, Arima is situated only 30 km northeast of the epicenter of the 1995 Kobe earthquake, and historical records have shown sudden temperature increases after earthquakes in this area[19]. We recently acquired the latest isotope data while compiling past data of more than half a century to identify meteoric and lithospheric components in hot spring waters and then verified that the lithospheric component is slab-derived water by comparing its isotopic signatures with numerical predictions. Finally, we show secular variations in the fraction of slab-derived water and quantify its amount replenished in conjunction with the earthquake.

Results

Two end-members of hot spring water

As shown by previous studies[15,16,18], the δ^{18}O-δ^2H relationships in the seven selected hot spring waters are almost linear (Fig. 2, Supplementary Table 2), and the slope (=1.345 ± 0.070) of the regression line is far smaller than the slope (=8.552) of the local meteoric water line (LMWL). Since such a linear correlation is found for the relationship between the Cl^- concentration and δ^2H or δ^{18}O[15,16,18] (Eqs. (2) and (3) in "Methods", Supplementary Table 3), the regression line (Eq. (1) in "Methods") for hot spring waters in the δ^{18}O-δ^2H space is regarded as the mixing line (MXL) between two end-members rather than the trend in the isotope shift from meteoric water[20]. Both the δ^2H (= −52.1‰) and δ^{18}O (= −8.12‰) values of the meteoric end-member coincide with those of cold mineral (carbonated and Rn-containing) springs and are slightly lower than those of nearby rivers (Supplementary Table 2), indicating that the mean recharge elevation of the meteoric component of the springs is greater than the catchment mean elevation of the rivers[21]. On the other hand, the non-meteoric end-member is regarded as lithospheric water (including slab-derived water), and its isotopic signature is determined to be δ^2H = −29.0 and δ^{18}O = +8.93 as the intersection point of the MXL

[1]Institute of Life and Environmental Sciences, University of Tsukuba, Tennodai 1-1-1, Tsukuba, Ibaraki, 305-8572, Japan. [2]Graduate School of Life and Environmental Sciences, University of Tsukuba, Tennodai 1-1-1, Tsukuba, Ibaraki, 305-8572, Japan. ✉e-mail: tyam@geoenv.tsukuba.ac.jp

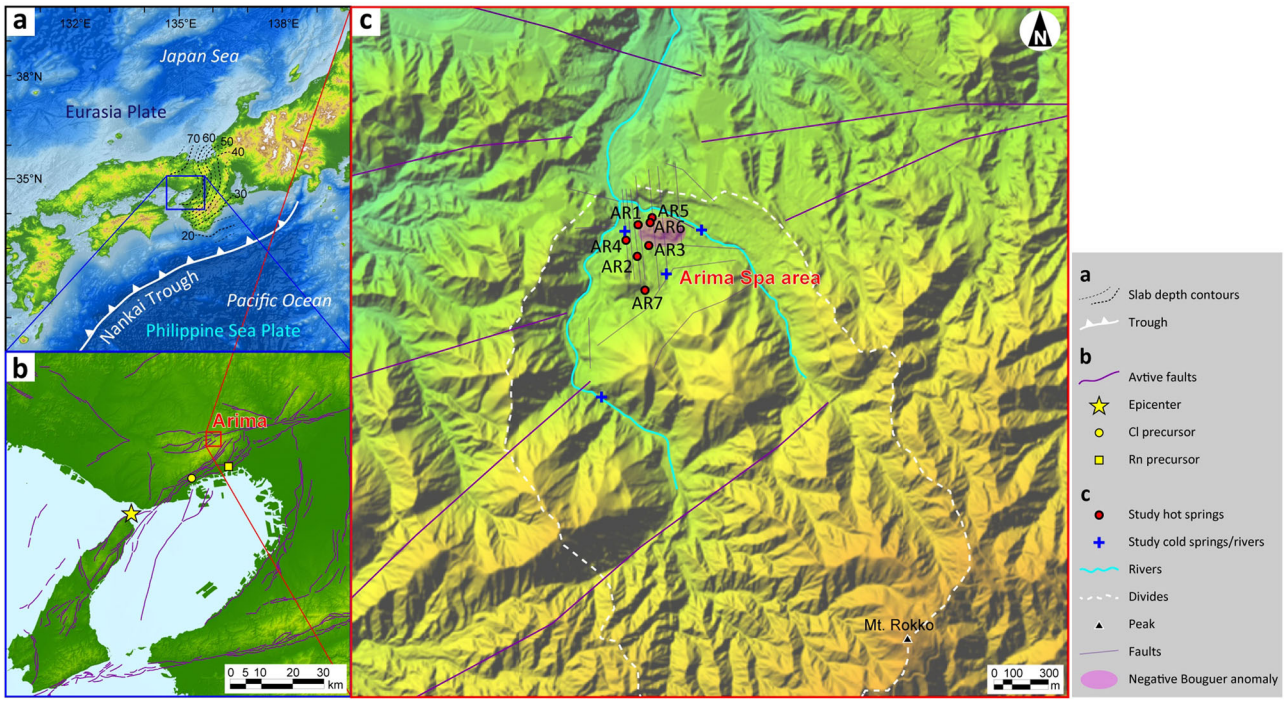

Fig. 1 | Location and tectonic setting of Arima hot springs. a Index map showing western Japan and Nankai Trough with contours to top of the Philippine Sea slab[25] (black dashed lines). **b** Map showing locations of the epicenter of 1995 Kobe earthquake (yellow star), monitoring sites of precursory changes in Cl[33] (yellow circle) and Rn[34] (yellow square), and active faults[53] (purple lines). **c** Map showing sampling sites of hot springs (red circles; AR1-AR7) and cold springs/rivers (blue crosses) with divides for nearby rivers (white dashed lines), active[53]/nonactive[54] faults (thick/thin purple lines), and negative Bouguer anomaly domain[30] (pink ellipse). (**a**) and (**b**) were created using the ArcGIS Pro 3.1.2 (Esri Inc.) with digital elevation model of the ETOPO 2022 15 Arc-Second Global Relief Model[55] (in **a**) and the Japan Flow Direction Map[56] (in **b**). (**c**) was created by editing GSI Tiles (elevation) at Geospatial Information Authority of Japan website (https://maps.gsi.go.jp/vector/#13.048/34.7846/135.219595/&ls=vstd%7Crelief%7Crelief_free&disp=101&d=l&reliefdata=35G0000FFGAG0095FFGFAG00EEFFG12CG91FF00G1F4GFFFF00G3E8GFF8C00GGFF4400).

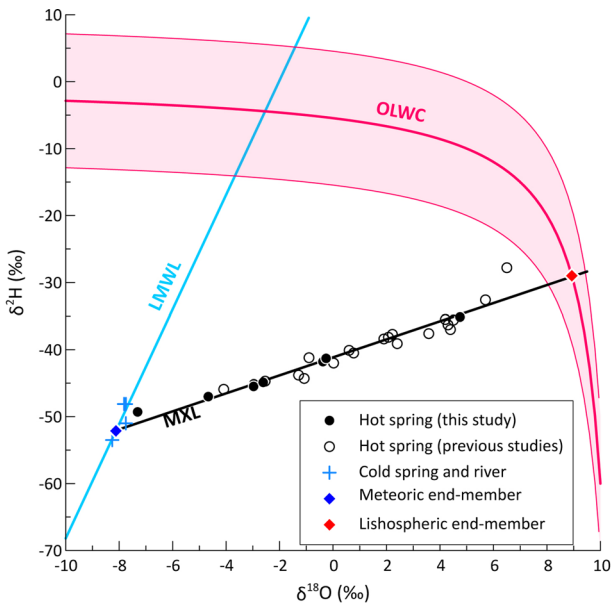

Fig. 2 | Measured isotope data in the $\delta^{18}O$-$\delta^{2}H$ space. LMWL, local meteoric water line; MXL, mixing line; OLWC, ocean-origin lithospheric water curve. Shaded zone represents uncertainty range of OLWC[22].

and the ocean-origin lithospheric water curve (OLWC)[22]. This newly determined isotopic signature of the lithospheric end-member is similar to but updates past estimates for $\delta^{2}H$ (−25 to −30‰[15], −32‰[16], and −33‰[18]) and $\delta^{18}O$ (+8‰[15], +10‰[16], and +6‰[18]).

Origin of lithospheric end-members

Some past studies have inferred that the lithospheric component of Arima hot springs consists of slab-derived fluids. This inference is grounded in the unique $\delta^{2}H$ and $\delta^{18}O$ values that resemble those of magmatic water, $^{3}He/^{4}He$ ratios equivalent to those of mantle helium[18], Li/Cl ratios reflecting high-temperature reactions[23], and extraordinarily low $\delta^{88/86}Sr$ values[24]. However, the H isotopic signature of the lithospheric component has not evidently matched the numerical prediction for water derived from the Philippine Sea slab at depths >60 km (i.e., the depths estimated for Arima[25]); rather, it has matched that for the Pacific slab at the same depths[18].

Unlike the previous study, comparisons between the H and O isotopic signatures of lithospheric end-members and those of slab-derived water numerically predicted by our improved model of water isotope evolution under conditions of Philippine Sea slab subduction[22] show very good agreement (Fig. 3). The predicted temperature range (500–600 °C) of the slab top beneath Arima corresponds to temperatures suitable for dehydration by metamorphic processes[1,26]. These results show that the lithospheric component contained in the Arima hot springs was indeed derived from the Philippine Sea slab. In addition, it is confirmed that the ascending water from the slab through wedge mantle is not affected by isotopic re-equilibration with mantle peridotites, probably owing to the water/rock ratio (i.e., the total mass of water successively flowing through preferential paths versus the limited mass of rock that reacts with the flow) being large enough to fully adjust the isotopic signature of the rock to that of the water[27,28].

Secular variation in the slab-derived water fraction

The latest isotopic signatures of the hot springs are closer to the meteoric end-member than they were in the past (Fig. 2). In six out of seven hot springs, the fraction of slab-derived water (F_{sdw}), which is estimated from

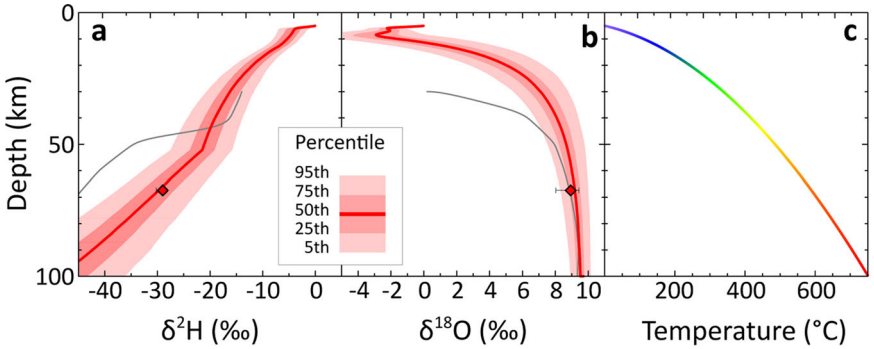

Fig. 3 | Comparison between isotopic signatures of the lithospheric end-member and those predicted for water in subducting Philippine Sea slab. **a**, **b** The δ^2H (**a**) and $\delta^{18}O$ (**b**) versus the depth (below sea level) of Philippine Sea slab top. **c** Predicted depth profile of the slab top temperature. Red diamonds (error bars) represent isotopic signatures (uncertainties) of the lithospheric end-member of the Arima hot spring waters. Prediction results shown as red-shaded zones are from the Monte Carlo simulation (1000 runs in each panel) considering uncertainties in model parameters[22]. Gray lines represent predictions in a previous study[18].

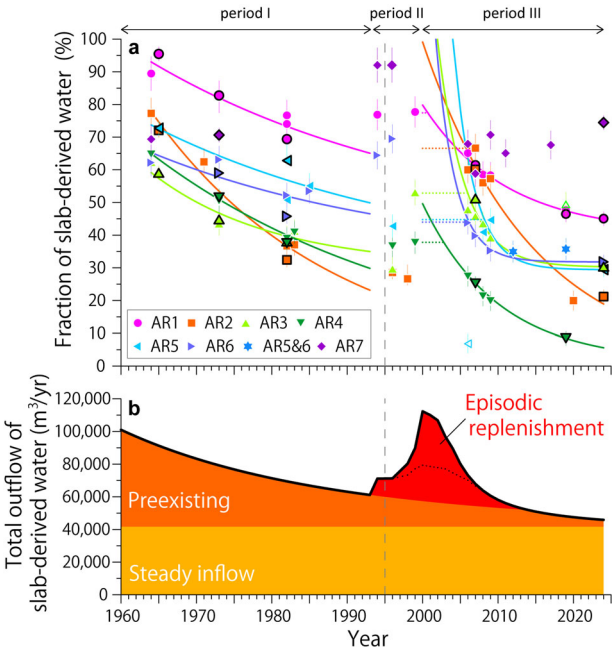

Fig. 4 | Secular variation in slab-derived water. **a** Variation in the fraction of slab-derived water (F_{sdw}) in the seven hot springs (AR1-AR7). Colored symbols outlined (non-outlined) in black show estimations from isotope (Cl) data. Approximated, exponential asymptotic curves (excluding AR7) are given as colored solid lines. Open symbols represent two outliers that are not used for the approximation. Error bars represent non-systematic uncertainties given by Eq. (9) in "Methods", and dashed vertical line shows the year of the Kobe earthquake occurrence. Colored dotted-lines represent the maximum estimated F_{sdw} after the earthquake as the lower limits of interpolated F_{sdw} at the former part of period III. Figures for each spring are given as Supplementary Fig. 1. **b** Variation of total outflow of slab-derived water through seven hot springs. Components of steady inflow, pre-existing (computed using Eq. (13) with the reservoir capacity, V, for Period I), and episodic replenishment (as residual) are shown. Dotted line represents the lower limits of the estimated total outflow.

mixing analysis using isotope data (including those converted from Cl data using Eqs. (2) and (3); Supplementary Table 4), shows exponential decay during period I (1960–1993) before the 1995 earthquake (Fig. 4a). This suggests that semi-finite amounts of slab-derived water are gradually diluted by meteoric water over time after deep borehole drilling (more than 200 m deep) for the current hot springs was performed in the 1940–1960s. At the same time, F_{sdw} tends to approach a constant value (not always zero), indicating a small steady supply of slab-derived water. The inconsistency in the values of F_{sdw} and their temporal variation among the springs imply the existence of multiple reservoirs with less water interchange. Seismic data support a high crack density at depths of ~18 km beneath the Arima area[29], and at more local scales, negative Bouguer anomalies are observed around the study springs[30] (Fig. 1c), supporting abundant cracks with large void spaces.

In period II (1994–1999; i.e., immediately before and after the earthquake), the F_{sdw} temporarily increases and then declines again exponentially in the subsequent period III (2000–2024). All these temporary surges in F_{sdw} are attributable to episodic replenishment of slab-derived water to the reservoirs, while the magnitude, timing of initiation, and duration of the increase differ among the springs. Historical documents have mentioned sudden increases in water temperature at Arima hot springs after intense earthquakes in 1596, 1854, 1899, and 1916[19]. In particular, it is estimated that the water temperature increased from approximately 40 to 90 °C after the 1596 earthquake. In addition, the temperature increase after the 1899 earthquake was accompanied by doubled outflow in the subsequent months. These facts suggest that earthquakes can episodically replenish very hot, slab-derived water into reservoirs, although the temperature increase due to earthquakes became unobvious after the deep borehole drilling because the ordinary temperature nearly reached the boiling point.

At the exceptional hot spring AR7, an increase in F_{sdw} in conjunction with the earthquake is also found, while it does not show obvious exponential decay and remains relatively high. This implies that at AR7, the steady inflow of slab-derived water to the reservoir (I_{sdw}) is relatively large compared to the capacity of the reservoir (V) and/or spring outflow (O) as mixtures of meteoric and slab-derived components.

Quantifying episodically replenished water

Assuming constant V and O during a period in question, the decay constant of F_{sdw} corresponds to the turnover time ($=V/O$)[31,32]. The estimated turnover time from a 'mixing reservoir' model (see "Methods") with curve fitting by an asymptotic exponential function for each spring (AR1-AR6) is 31.3 (±8.3) years on average (±SD) in period I and then decreases to 7.4 (± 4.7) years in period III (Supplementary Table 5, Supplementary Fig. 1). Using the mean O throughout all the periods at each of the springs (because no obvious change in O is observed between the two periods), the total capacity of the reservoirs is estimated to be approximately 3.3×10^6 m³ in period I and 7.6×10^5 m³ in period III. Assuming the reservoir capacity of 10^6 m³, horizontal cross-sectional area of 10^4 m² and average porosity of 0.1 as rough estimates yields their average depth of about 1000 m. The decrease in the reservoir capacity likely reflects either a reduction in void space or shrinkage of the depth zone where slab-derived water mixes with meteoric water (in other words, expansion of the zone that is saturated with slab-derived water) or both. Despite a constant O, the outflow of slab-derived water increased to nearly twice the amount at the 1993 level due to episodic replenishment (Fig. 4b). In total, 4.2×10^5 m³ of slab-derived water is estimated to have been episodically replenished in conjunction with the earthquake. However, the approximated (or extrapolated) F_{sdw} at the former part of period III may be somewhat overestimated. If we assume the maximum estimated F_{sdw} after the earthquake as the lower limits of approximated values at the period, the total amount of the episodic replenishment is reduced to 2.6×10^5 m³. In either case, although these amounts are relatively small compared to the slab-derived fluid storage (10^6–10^8 m³) involved in the earthquake swarm

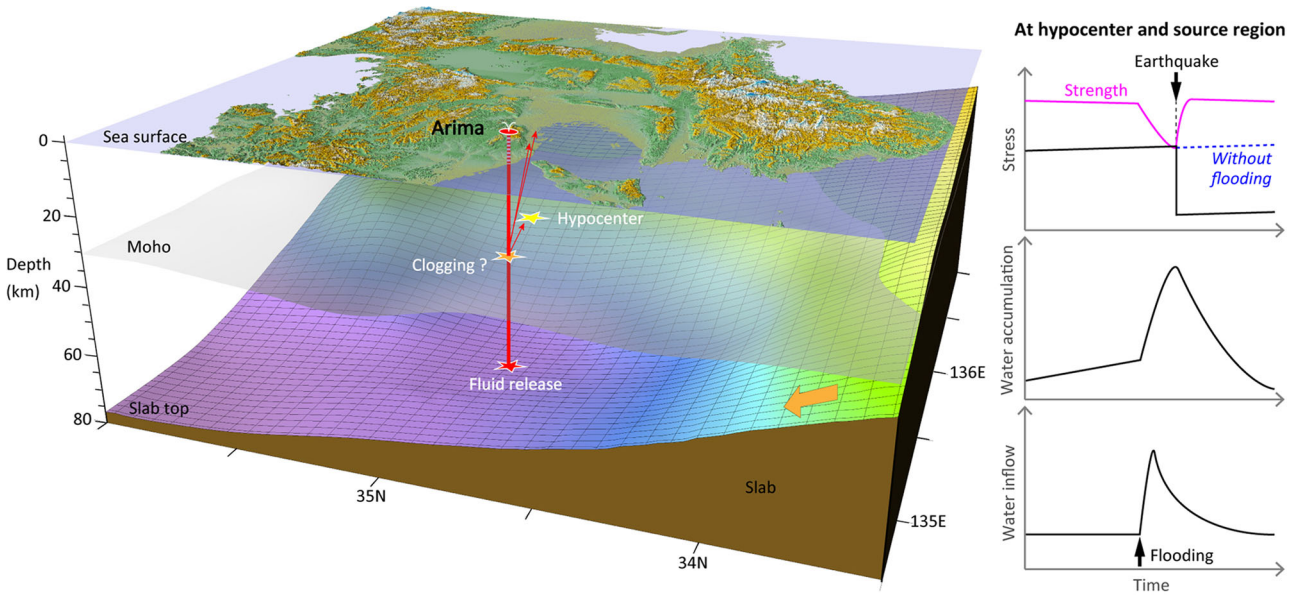

Fig. 5 | Conceptual model of the flooding of slab-derived water. This was created using the Surfer 24.3.218 (Golden Software, LLC) with the data of the land surface elevation[55], the Moho depth[57], and the slab top depth[25].

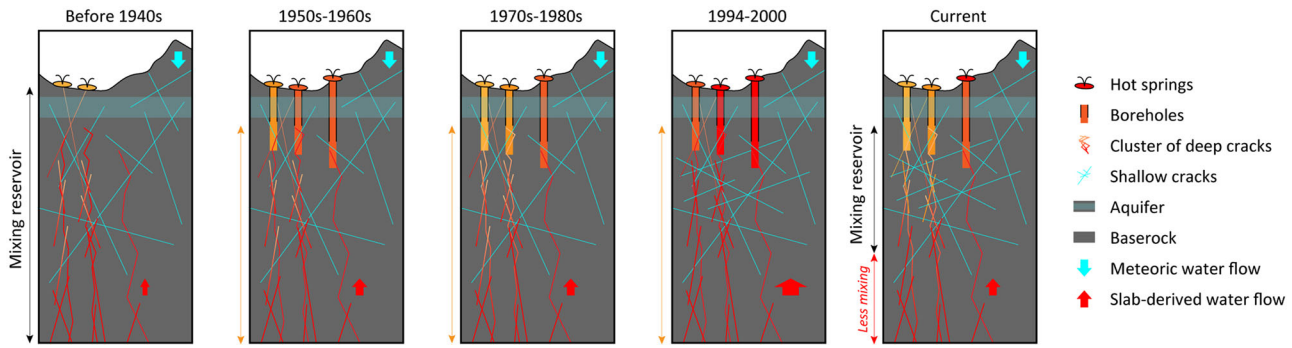

Fig. 6 | Conceptual model of slab-derived water upwelling and mixing.

associated with the 2011 Tohoku earthquake (M_w9.0)[10], the spatiotemporal density of the flow is considerably high at Arima.

Note that we excluded two data points (i.e., at AR5 in 2006 and at AR3 in 2019; represented by open symbols in Fig. 4a) from the curve fitting of the F_{sdw} decay. The former is accompanied by an extraordinarily low temperature (45.1 °C) compared to the ordinary temperature at AR5 (>90 °C) due to partial clogging of the permeable borehole wall by precipitates that inhibit the inflow of slab-derived water but not meteoric water inflow. In contrast, the latter is accompanied by a higher temperature (100.5 °C) and several times greater outflow than ordinary values (Supplementary Table 4). This irregular surge in F_{sdw} occurred immediately after dredging inside the borehole, indicating an enhanced inflow of slab-derived water that had been inhibited. These two cases suggest that changes in the borehole condition affect only short-term changes in F_{sdw}.

Discussion

The most interesting and debatable point in our results is that increases in F_{sdw} in the hot springs of AR1, AR6, and AR7 preceded the occurrence of the earthquake. It has been reported that the concentrations of Cl (20 km northeast of the epicenter and 10 km southwest of Arima; yellow circle in Fig. 1b)[33] and Rn (30 km northeast of the epicenter and 10 km southeast of Arima; yellow square in Fig. 1b)[34] in deep groundwater increased 3 to 5 months prior to the earthquake. H and O isotopic changes in groundwater as precursors to earthquakes have also been reported in other regions, for instance, Hafralækur in northern Iceland[35] and Tottori in western Japan[36]. Overpressurized fluids are often considered potential triggers for fault movement[4,5]. Therefore, it is highly likely that increases in F_{sdw} were also the precursors to the 1995 Kobe earthquake although we cannot specify when F_{sdw} started to increase because of the coarse measurement intervals. On the other hand, increases in F_{sdw} at AR2, AR3, and AR5 lag one or more years behind the main shock. Such large and variable time lags are distinct from those of other hydrogeochemical precursors and postseismic responses[37,38].

We infer that the earthquake and episodic replenishment of slab-derived water (as well as precursory changes in groundwater Cl and Rn) were both induced by a flood-like release of water from the slab (>60 km deep) or by bursting of clogged flow paths from the slab to the hypocenter (~18 km deep). Increase in water flow can propagate faster than the actual flow velocity by the piston-like flow (or called translatory flow; i.e., upstream waters push out downstream waters). Water inflow and accumulation at the source region including the hypocenter reduced the apparent friction coefficient and thus the fault strength, resulting in the earthquake; then, the seismicity facilitated further upwards migration of the slab-derived water (Figs. 5 and 6). If there had been no flooding, the earthquake might have occurred later. The slab-derived water and meteoric water are mixing in a network of the cracks (down to ca. 1000 m) as well as in boreholes. Isotope data suggest that the mean recharge elevation of the meteoric component of the hot springs is greater than the catchment mean elevation for adjacent

rivers, as mentioned at "Two end-members of hot spring", suggesting that the hydraulic head of meteoric water is higher than the ground surface at the hot spring sites. In addition, as mentioned at "Water budget analysis using the mixing reservoir model" in Methods, the hot springs are naturally or artificially gas-lifted, and static water level in the borehole is not always above the ground surface. Therefore, meteoric waters can mix with slab-derived waters. Before 1940s, hot springs were naturally flowing (without borehole drilling), and the meteoric component was dominated in shallower depth zones. On the other hand, the fraction of hot, slab-derived component was kept high in deeper zones. In 1950–60s the drilling of deep boreholes enabled outflow of waters having high temperature and high fraction of slab-derived component, making static level lower within the boreholes. This enlarged the influx of the meteoric water and diluted slab-derived water during 1970–80s. Flooding of slab-derived waters in the former 1990s replenished the mixing reservoirs with new slab-derived waters, and then they are still being diluted (Fig. 6).

A previous study on Arima hot springs argued that slab-derived fluid is originally under supercritical condition[39]. If that is correct, it will make it easier to explain the rapid and widespread movement of slab-derived fluid. However, some other studies suggested that the fluid at depths >83 km[40] or at temperatures >650 °C[41] is under supercritical condition. In our computation, predicted temperatures at the slab top beneath Arima (67.4 km depth) ranges from 500 to 600 °C. In addition, slab-derived fluid that reaches near the Earth's surface does not retain its original chemical composition (Supplementary Table 6), unlike fluid inclusions in minerals. Therefore, we cannot conclude whether slab-derived fluid that is contained in Arima hot spring waters was originally under supercritical condition or not. Even without assuming a supercritical fluid, rapid flood propagation can be explained by piston-like flow.

Our results indicate that large earthquakes do not strike anywhere[7,8] and anytime but they are more likely to occur at the time and place where the flooding of slab-derived water happens. A situation similar to the 1995 Kobe earthquake can be found in the 1965–1967 earthquake swarm (the highest $M_w = 5.4$) at Matsushiro, central Japan, where more than 700,000 earthquakes were observed together with a vast volume of enhanced outflows (~10^7 m^3/yr) of saline water oversaturated with CO_2 at a hot spring[42,43]. Although the saline water involved in this swarm has been postulated to be of magma origin[43,44], our recent study[22] showed that it is also derived from the Philippine Sea slab (in the original paper, Na2 and Na3 correspond to hot springs at Matsushiro). The similarity between Arima and Matsushiro highlights the importance of hot springs as outlets of slab-derived water. Exploring such hydrologically slab-connected hot springs across subduction zones and their long-term, frequent monitoring will deepen and broaden our understanding of the ultradeep water cycle and its causal relationship with earthquakes.

Methods

Sampling, isotopic analysis, and data compilation

At Arima, there are more than forty source springs, including hot and/or mineral springs, for spas. We collected water samples from seven typical hot springs and two cold mineral springs as well as from two nearby rivers in August 2019 and/or January 2024 (Supplementary Table 1). Hydrogen and oxygen stable isotope ratios in the water samples were measured by cavity ring-down laser absorption spectroscopy (CRDS) using an L2130-i instrument (Picarro Inc., Santa Clara, CA, USA) at the Center for Research in Radiation, Isotopes, and Earth System Sciences (CRiES), University of Tsukuba. Two working standards, calibrated against three international standards (Vienna Standard Mean Ocean Water, Standard Light Antarctic Precipitation, and Greenland Ice Sheet Precipitation), were analyzed with samples for validation (or calibration if necessary). The measurement errors are ±0.25‰ for δ^2H and ±0.05‰ for $\delta^{18}O$. We also assembled a previously measured dataset of both δ^2H and $\delta^{18}O$ (with accuracy of ±1‰ and ±0.1‰, respectively) in the studied hot springs (Supplementary Table 3). Additionally, to increase the temporal resolution of the isotopic data, Cl data (with accuracy of about ±100 mg/kg) as proxies were compiled based on previous studies[45–49] and those provided by spring owners (Supplementary Tables 4 and 6; the analysis of Cl content is conducted in accordance with the guidelines established by the Japanese government). The regression lines for the $\delta^{18}O$-δ^2H, Cl-δ^2H, and Cl-$\delta^{18}O$ relationships in the hot springs are given as

$$\delta^2H = 1.345 \times \delta^{18}O - 41.15 \, (r^2 = 0.937) \quad (1)$$

$$\delta^2H = 5.011 \times 10^{-4} \times Cl - 51.81 \, (r^2 = 0.870) \quad (2)$$

$$\delta^{18}O = 3.483 \times 10^{-4} \times Cl - 7.26 \, (r^2 = 0.985) \quad (3)$$

where Cl is the chloride ion concentration (mg/kg). The regression lines for the $\delta^{18}O$-δ^2H relationships in the cold mineral springs and rivers, which represent the local meteoric water line (LMWL) at Arima, are expressed as follows.

$$\delta^2H = 8.552 \times \delta^{18}O + 17.32 \, (r^2 = 0.660) \quad (4)$$

Although Eq. (4) is derived from limited data ($n = 4$) and its determination coefficient (r^2) is not high enough, it is close to the LMWL ($\delta^2H = 8 \times \delta^{18}O + 17$) at Okayama (120 km west of Arima)[50] and thus considered confident.

Mixing analysis of hot spring water

The isotopic evolution of ocean-origin lithospheric waters (including not only slab-derived water but also so-called fossil seawater, metamorphic water, and magmatic water, as found in subseafloor pore water, submarine mud volcano pore water, coastal oil-field brine and volcanic steam) in the $\delta^{18}O$-δ^2H space can be approximated by the ocean-origin lithospheric water curve (OLWC)[22], as expressed by

$$\delta^2H = 60/(\delta^{18}O - \delta^{18}O_{fin}) + \delta^2H_{off} \quad (5)$$

where $\delta^{18}O_{fin} = 11 \pm 1$ and $\delta^2H_{off} = 0 \pm 10$. The isotopic signature of the lithospheric end-member can be obtained as the coordinate of the intersection point of the OLWC and the mixing line (MXL) in the $\delta^{18}O$-δ^2H space as follows:

$$\delta^{18}O = \left[-i + \delta^2H_{off} + s\delta^{18}O_{fin} - \sqrt{\left(i - \delta^2H_{off} - s\delta^{18}O_{fin}\right)^2 - 4s\left(-i\delta^{18}O_{fin} + \delta^{18}O_{fin}\delta^2H_{off} - 60\right)}\right]/2s \quad (6)$$

$$\delta^2H = s\delta^{18}O + i \quad (7)$$

where s and i are the slope and intercept of the MXL (i.e., Eq. (1)), respectively. Similarly, the coordinates of the intersection points of the LMWL and MXL indicate the isotopic signature of the meteoric end-member. The fraction of slab-derived water (i.e., the most likely lithospheric component in the present study) is obtained as

$$F_{sdw} = (\delta_{hs} - \delta_{mw})/(\delta_{lw} - \delta_{mw}) \quad (8)$$

where δ is δ^2H or $\delta^{18}O$ and the subscripts hs, mw, and lw denote the hot spring, meteoric end-member, and lithospheric end-member, respectively. We adopted the mean of the δ^2H-based and $\delta^{18}O$-based values, even when the Cl data were converted to δ^2H and $\delta^{18}O$ using Eqs. (2) and (3). Expected

errors in F_{sdw} (ε_F) is given as

$$\varepsilon_F = \varepsilon_\delta/(\delta_{lw} - \delta_{mw}) \quad (9)$$

where ε_δ is the measurement errors in δ^2H (=1‰) or $\delta^{18}O$ (=0.1‰). In case where δ values are converted from Cl, the ε_δ is given as

$$\varepsilon_\delta = \sqrt{(\varepsilon_{Cl} \cdot a)^2 + (Cl \cdot \varepsilon_a)^2 + \varepsilon_b{}^2} \quad (10)$$

where ε_{Cl} is the measurement errors in Cl concentrations (=100 mg kg^{-1}), a is the slope of the Cl-δ regression lines, ε_a and ε_b are the standard errors of a and b (the intercept of the regression lines), respectively. The Cl concentrations in the meteoric end-member can vary, resulting in uncertainties in the Cl-δ regression lines and thus errors in F_{sdw} estimation. Such an effect as well as errors in Cl measurements can be considered by Eq. (10).

Numerical prediction of the isotopic signature of slab-derived water

To identify the origin of the lithospheric component in hot spring waters, we numerically predicted the isotopic signature of water in the subducting Philippine Sea slab using a model of H and O isotope evolution[22]. Unlike the previous Rayleigh-type model[18], our model computes the nonequilibrium exchange of hydrogen/oxygen isotopes among pools of pore water, interlayer water in clay particles (including adsorbed water on mineral surfaces), OH groups of hydrous minerals, and O atoms constituting mineral crystals. The temperature of the slab and the depth of the slab top surface along the horizontal distance from the Nankai Trough were given at every time step (=10,000 years) by empirical equations that approximate the simulation results for the subduction of the Philippine Sea slab[26]. To consider uncertainties in the model parameters, a Monte Carlo simulation result of 1000 runs was employed. To compare the prediction results and the isotopic signatures of lithospheric end-members, we estimated the depth of the Philippine Sea slab surface beneath the Arima area by interpolating depth contours from a previous study[25] with ordinary kriging. Although there is little difference in geometry of Philippine Sea slab among literatures[51], the difference in estimated slab-depths at Arima is within some 1 km.

Water budget analysis using the mixing reservoir model

The ancient hot springs in Arima are naturally flowing. Since the 1940s, deep wells for the current hot springs have been drilled, and they were originally the geysers due to a (natural CO_2) gas-lift effect[45]. Then, inner pipes with enlarged diameters with deep ends were introduced into boreholes to increase the effect; hot water nearly continuously flows out (even if the static water level in the borehole is below the ground), while the intermittent nature of outflows with variable temperatures still persists (and in some springs, water is sometimes artificially gas-lifted using compressed air). Based on these characteristics, it has been inferred that slab-derived water moves from depth towards boreholes through a cluster of interconnected cracks, which form along faults and/or around intrusive bodies of igneous rock[17,52].

The cluster of such cracks can be regarded as a water reservoir, where slab-derived water and meteoric water mix and a hot spring corresponds to its outlet. The temporal change in the storage amount of slab-derived water (S_{sdw}) within the mixing reservoir is expressed as

$$dS_{sdw}/dt = I_{sdw} - OF_{sdw} \quad (11)$$

where t is the time, I_{sdw} is the inflow of slab-derived water into the reservoir, and O is the outflow as a mixture of the slab-derived component and meteoric component. The temporal change in F_{sdw} as a spatial mean within a cluster of cracks is given as follows.

$$dF_{sdw}/dt = (I_{sdw} - OF_{sdw})/V \quad (12)$$

Under the assumptions of a constant V, I_{sdw}, and O during a period in question, integrating Eq. (12) yields

$$F_{sdw} = (F_0 - I_{sdw}/O)\exp[-(O/V)t] + I_{sdw}/O \quad (13)$$

where F_0 is the initial (i.e., $t = 0$) value of F_{sdw}. If we approximate the temporal change in F_{sdw} by an exponential asymptotic function, $F_{sdw} = c + b\exp(at)$, we obtain $I_{sdw} = cO$, $F_0 = b + c$, $\tau = -a^{-1}$, and $V = \tau O$, where τ is the decay constant or the turnover time (Supplementary Table 5). In the present study, we assumed that I_{sdw} and O remained constant throughout all the periods. For each spring, we obtained the value of I_{sdw}/O that maximizes the sum of r^2 for periods I and III using the logarithmic conversion of Eq. (13) and its linear regression. For period II, we reconstructed F_{sdw} values via linear interpolation as a first approximation (Supplementary Fig. 1). The use of parameters in period I for extrapolating the exponential decay in F_{sdw} (regardless of the occurrence of the earthquake) provides the hypothetical outflow of pre-existing slab-derived water. Thus, the difference between the actual and hypothetical outflows represents the outflow of the episodically replenished component (Fig. 4b).

Data availability

The measured isotope data and related information are provided in Supplementary Tables 1–6. Those as well as source data for figures are available at https://doi.org/10.6084/m9.figshare.26264603.

Code availability

An Excel Macro (VBA) code for executing the isotopic evolution model[22] is available at https://www.geoenv.tsukuba.ac.jp/~tyam/iem/.

Received: 4 April 2024; Accepted: 6 August 2024;
Published online: 02 September 2024

References

1. Hyndman, R. D. & Peacock, S. M. Serpentinization of the forearc mantle. *Earth Planet. Sci. Lett.* **212**, 417–432 (2003).
2. Stern, R. J. Subduction zones. *Rev. Geophys.* **40**, 1012 (2002).
3. Peslier, A. H., Schönbächler, M., Busemann, H. & Karato, S. Water in the Earth's interior: distribution and origin. *Space Sci. Rev.* **212**, 743–810 (2017).
4. Julve, J. et al. Recurrence time and size of Chilean earthquakes influenced by geological structure. *Nat. Geosci.* **17**, 79–87 (2024).
5. Zhao, D., Kanamori, H., Negishi, H. & Wiens, D. Tomography of the source area of the 1995 Kobe earthquake: evidence for fluids at the hypocenter? *Science* **274**, 1891–1894 (1996).
6. Di Luccio, F., Ventura, G., Di Giovambattista, R., Piscini, A. & Cinti, F. R. Normal faults and thrusts reactivated by deep fluids: the 6 April 2009 M_w 6.3 L'Aquila earthquake, central Italy. *J. Geophys. Res.* **115**, B06315 (2010).
7. Zhao, D., Ochi, F., Hasegawa, A. & Yamamoto, A. Evidence for the location and cause of large crustal earthquakes in Japan. *J. Geophys. Res.* **105**, 13579–13594 (2000).
8. Zhao, D., Mishra, O. P. & Sanda, R. Influence of fluids and magma on earthquakes: seismological evidence. *Phys. Earth Planet. Inter.* **132**, 249–267 (2002).
9. Halpaap, F. et al. Earthquakes track subduction fluids from slab source to mantle wedge sink. *Sci. Adv* **5**, eaav7369 (2019).
10. Mukuhira, Y., Uno, M. & Yoshida, K. Slab-derived fluid storage in the crust elucidated by earthquake swarm. *Commun. Earth Environ* **3**, 286 (2022).

11. Nishimura, T., Hiramatsu, Y. & Ohta, Y. Episodic transient deformation revealed by the analysis of multiple GNSS networks in the Noto Peninsula, central Japan. *Sci. Rep.* **13**, 8381 (2023).
12. Nakajima, J. Crustal structure beneath earthquake swarm in the Noto Peninsula, Japan. *Earth Planets Space* **74**, 160 (2022).
13. Yoshida, K. et al. Upward earthquake swarm migration in the northeastern Noto Peninsula, Japan, initiated from a deep ring-shaped cluster: possibility of fluid leakage from a hidden magma system. *J. Geophys. Res. Solid Earth* **128**, e2022JB026047 (2023).
14. van Keken, P. E., Hacker, B. R., Syracuse, E. M. & Abers, G. A. Subduction factory: 4. Depth-dependent flux of H_2O from subducting slabs worldwide. *J. Geophys. Res.* **116**, B01401 (2011).
15. Matsubaya, O., Sakai, H., Kusachi, I. & Satake, H. Hydrogen and oxygen isotopic ratios and major element chemistry of Japanese thermal water systems. *Geochem. J.* **7**, 123–151 (1973).
16. Masuda, H., Sakai, H., Chiba, H. & Tsurumaki, M. Geochemical characteristics of Na-Ca-Cl-HCO_3 type waters in Arima and its vicinity in the western Kinki district, Japan. *Geochem. J.* **19**, 149–162 (1985).
17. Nishimura, S., Katsura, I. & Nishida, J. Geological structure of Arima hot-spring. *J. Hot Spring Sci.* **56**, 3–15 (2006).
18. Kusuda, C., Iwamori, H., Nakamura, H., Kazahaya, K. & Morikawa, N. Arima hot spring waters as a deep-seated brine from subducting slab. *Earth Planets Space* **66**, 119 (2014).
19. Masuda, H. Arima hot spring—a window of the Earth's deep. *J. Hot Spring Sci.* **61**, 203–221 (2011).
20. Craig, H. In *Nuclear Geology on Geothermal Areas* 17–53 (CNR, 1963).
21. Yamanaka, T. & Yamada, Y. Regional assessment of recharge elevation of tap water sources using the isoscape approach. *Mt. Res. Dev.* **37**, 198–205 (2017).
22. Adachi, I. & Yamanaka, T. Isotopic evolutionary track of water due to interaction with rocks and its use for tracing water cycle through the lithosphere. *J. Hydrol.* **628**, 130589 (2024).
23. Kazahaya, K. et al. Spatial distribution and feature of slab-related deep-seated fluid in SW Japan. *J. Jpn. Assoc. Hydrol. Sci.* **44**, 3–16 (2014).
24. Kani, T. et al. Strontium isotope characteristics ($\delta^{88/86}$Sr, ^{87}Sr/^{86}Sr) of Arima-type brines originated from slab-fluids. *Geophys. Res. Lett.* **50**, e2022GL100309 (2023).
25. Ide, S., Shiomi, K., Mochizuki, K., Tonegawa, T. & Kimura, G. Split Philippine Sea plate beneath Japan. *Geophys. Res. Lett.* **37**, L21304 (2010).
26. Peacock, S. M. & Wang, K. Seismic consequences of warm versus cool subduction metamorphism: examples from southwest and northeast Japan. *Science* **286**, 937–939 (1999).
27. Clayton, R. N. & Steiner, A. Oxygen isotope studies of the geothermal system at Wairakei, New Zealand. *Geochim. Cosmochim. Acta* **39**, 1179–1186 (1975).
28. Sakai, R., Kusakabe, M., Noto, M. & Ishii, T. Origin of waters responsible for serpentinization of the Izu-Ogasawara-Mariana forearc seamounts in view of hydrogen and oxygen isotope ratios. *Earth Planet. Sci. Lett.* **100**, 291–303 (1990).
29. Zhao, D. & Mizuno, T. Crack density and saturation rate in the 1995 Kobe earthquake region. *Geophys. Res. Lett.* **26**, 3213–3216 (1999).
30. Nishimura, S., Katsura, I., Nishida, J., Kawasaki, I. & Jyomori, N. On the hot spring reservoir at Arima hot spring field. *J. Hot Spring Sci* **65**, 14–24 (2015).
31. Bolin, B. & Rodhe, H. A note on the concepts of age distribution and transit time in natural waters. *Tellus* **25**, 58–62 (1973).
32. Yamanaka, T. *Tracing the Hydrological Cycle Using Environmental Isotopes* (Kyoritsu Shuppan, 2020).
33. Tsunogai, U. & Wakita, H. Precursory chemical changes in ground water: Kobe earthquake, Japan. *Science* **269**, 61–63 (1995).
34. Igarashi, G. et al. Ground-water radon anomaly before the Kobe earthquake in Japan. *Science* **269**, 60–61 (1995).
35. Skelton, A. et al. Changes in groundwater chemistry before two consecutive earthquakes in Iceland. *Nat. Geosci.* **7**, 752–756 (2014).
36. Onda, S. et al. Groundwater oxygen isotope anomaly before the M6.6 Tottori earthquake in Southwest Japan. *Sci. Rep.* **8**, 4800 (2018).
37. Tokunaga, T. Modeling of earthquake-induced hydrological changes and possible permeability enhancement due to the 17 January 1995 Kobe Earthquake, Japan. *J. Hydrol.* **223**, 221–229 (1999).
38. Hosono, T., Yamada, C., Manga, M., Wang, C.-Y. & Tanimizu, M. Stable isotopes show that earthquakes enhance permeability and release water from mountains. *Nat. Commun.* **11**, 2776 (2020).
39. Nishimura, S. High temperature hot springs and their geological structures of Kinki district, Japan. *J. Hot Spring Sci.* **60**, 481–491 (2011).
40. Kawamoto, T., Kanzaki, M., Mibe, K., Matsunaga, K. M. & Ono, S. Separation of supercritical slab-fluid and melt components in subduction zone magmatism. *PNAS* **109**, 18695–18700 (2012).
41. Ni, H., Zhang, L., Xiong, X., Mao, Z. & Wang, J. Supercritical fluids at subduction zones: evidence, formation condition, and physicochemical properties. *Earth Sci. Rev.* **167**, 62–71 (2017).
42. Tsuneishi, Y. & Nakamura, K. Fault associated with the Matsushiro swarm earthquake. *Bull. Earthquake Res. Inst. Univ. Tokyo* **48**, 29 (1970).
43. Cappa, F., Rutqvist, J. & Yamamoto, K. Modeling crustal deformation and rupture processes related to upwelling of deep CO_2-rich fluids during the 1965–1967 Matsushiro earthquake swarm in Japan. *J. Geophys. Res.* **114**, B10304 (2009).
44. Yoshida, N., Okusawa, T. & Tsukubahara, H. Origin of deep Matsushiro earthquake swarm fluid inferred from isotope ratios. *Zisin* **55**, 207–216 (2002).
45. Tsurumaki, M. *Report on the Geology and Hot Springs of Arima Hot Springs: Part 2* (Department of Planning and Development, 1964).
46. Teranishi, K., Isomura, K. & Yamamoto, K. The interaction between the brine-calcite in Arima and its vicinity of Hyogo Prefecture. *J. Hot Spring Sci.* **38**, 141–153 (1988).
47. Tsuji, H. et al. Determination of trace elements in Arima spring water by ICP-AES after coprecipitation with iron(III) hydroxide. *Bunseki Kagaku* **44**, 471–476 (1995).
48. Tsuji, H. et al. Studies of Arima type spring water in Arima spa of Hyogo Prefecture—for major and trace elements. *J. Hot Spring Sci.* **47**, 1–13 (1997).
49. Mashiko, T., Ohtsuka, A. & Takahashi, T. Monitoring for thermal water resource protection and characteristics of hot- and mineral-waters in Arima spa, Hyogo Prefecture. *J. Hot Spring Sci.* **62**, 144–167 (2012).
50. Yamamoto, M., Kitamura, T., Akagi, S., Furukawa, T. & Kusakabe, M. Hydrogen and oxygen isotope ratios of meteoric waters in Okayama Prefecture, Japan. *J. Jpn. Assoc. Groundwater Hydrol.* **35**, 107–112 (1993).
51. Zhao, D., Wang, J., Huang, Z. & Liu, X. Seismic structure and subduction dynamics of the western Japan arc. *Tectonophysics* **802**, 228743 (2021).
52. Nshimura, S. High temperature hot springs and their geological structures of Kinki District, Japan. *J. Hot Spring Sci.* **60**, 481–491 (2011).
53. National Institute of Advanced Industrial Science and Technology. Active Fault Database of Japan, February 28, 2012 version. Research Information Database DB095. https://gbank.gsj.jp/activefault/index_e_gmap.html (National Institute of Advanced Industrial Science and Technology, 2012).
54. Tawa, K. et al. Data on water temperatures of the Arima hotsprings—1961 to 1988. *Bull. Tokyo Gakugei Univ. Sect. 4* **41**, 201–215 (1989).
55. NOAA National Centers for Environmental Information. *ETOPO 2022 15 Arc-Second Global Relief Model*. https://doi.org/10.25921/fd45-gt74 (NOAA National Centers for Environmental Information, 2022).

56. Yamazaki, D., Togashi, S., Takeshima, A. & Sayama, T. High-resolution flow direction map of Japan. *J. Jpn. Soc. Civil Eng. (B1)* **74**, I_163–I_168 (2018). (5).
57. Matsubara, M., Sato, H., Ishiyama, T. & Van Horne, A. D. Configuration of the Moho discontinuity beneath the Japanese Islands derived from three-dimensional seismic tomography. *Tectonophysics* **710–711**, 97–107 (2016).

Acknowledgements

This work was supported by a Grant-in-Aid for Scientific Research (grant nos. 15H02957, 19H01370 & 24K00169) from Japan Society for the Promotion of Science. We thank owners/managers of individual studied spas for accepting the source water collection.

Author contributions

T.Y. designed and initiated the research, interpreted the data, and wrote the first draft of the paper. I.A. synthesized previous data, verified the analysis, and rewrote the paper.

Competing interests

The authors declare no competing interests.

Additional information

Supplementary information The online version contains supplementary material available at https://doi.org/10.1038/s43247-024-01606-1.

Correspondence and requests for materials should be addressed to Tsutomu Yamanaka.

Peer review information *Communications Earth & Environment* thanks the anonymous reviewers for their contribution to the peer review of this work. Primary Handling Editors: Evan Hastie and Carolina Ortiz Guerrero. A peer review file is available.